

## The rate of cellular hydrogen peroxide removal shows dependency on GSH: Mathematical insight into *in vivo* H<sub>2</sub>O<sub>2</sub> and GPx concentrations

CHIN F. NG<sup>1</sup>, FREYA Q. SCHAFER<sup>2</sup>, GARRY R. BUETTNER<sup>2</sup>, & V. G. J. RODGERS<sup>1</sup>

<sup>1</sup>Bioengineering Department, University of California, Riverside, CA 92521, USA, and <sup>2</sup>Free Radical and Radiation Biology Program & ESR Facility, Radiation Oncology, The University of Iowa, Iowa City, IA 52242-1101, USA

Accepted by Professor B. Halliwell

(Received 20 July 2007; in revised form 10 August 2007)

### Abstract

Although its concentration is generally not known, glutathione peroxidase-1 (GPx-1) is a key enzyme in the removal of hydrogen peroxide (H<sub>2</sub>O<sub>2</sub>) in biological systems. Extrapolating from kinetic results obtained *in vitro* using dilute, homogenous buffered solutions, it is generally accepted that the rate of elimination of H<sub>2</sub>O<sub>2</sub> *in vivo* by GPx is independent of glutathione concentration (GSH). To examine this doctrine, a mathematical analysis of a kinetic model for the removal of H<sub>2</sub>O<sub>2</sub> by GPx was undertaken to determine how the reaction species (H<sub>2</sub>O<sub>2</sub>, GSH, and GPx-1) influence the rate of removal of H<sub>2</sub>O<sub>2</sub>. Using both the traditional kinetic rate law approximation (classical model) and the generalized kinetic expression, the results show that the rate of removal of H<sub>2</sub>O<sub>2</sub> increases with initial GPx<sub>r</sub>, as expected, but is a function of both GPx<sub>r</sub> and GSH when the initial GPx<sub>r</sub> is less than H<sub>2</sub>O<sub>2</sub>. This simulation is supported by the biological observations of Li et al.. Using genetically altered human glioma cells in *in vitro* cell culture and in an *in vivo* tumour model, they inferred that the rate of removal of H<sub>2</sub>O<sub>2</sub> was a direct function of GPx activity × GSH (effective GPx activity). The predicted cellular average GPx<sub>r</sub> and H<sub>2</sub>O<sub>2</sub> for their study are approximately GPx<sub>r</sub> ≤ 1 μM and H<sub>2</sub>O<sub>2</sub> ≈ 5 μM based on available rate constants and an estimation of GSH. It was also found that results from the accepted kinetic rate law approximation significantly deviated from those obtained from the more generalized model in many cases that may be of physiological importance.

**Keywords:** Glutathione, glutathione peroxidase, hydrogen peroxide, mathematical modelling, kinetics

**Abbreviations:** C<sub>j</sub>, concentration of species *j*;  $\frac{dC_j}{dt}$ , rate of change of species *j*; DCFH<sub>2</sub>, 2',7'-dichlorodihydrofluorescein; GPx, glutathione peroxidase; GPx-1, classic (cytosolic) glutathione peroxidase; GPx<sub>o</sub>, oxidized glutathione peroxidase; GPx<sub>r</sub>, reduced glutathione peroxidase, the form that reacts with hydroperoxides; GS-GPx, glutathione-enzyme complex; GSH, glutathione; GSSG, glutathione disulphide; k<sub>j</sub>, reaction rate constant of reaction *j*; ODE, ordinary differential equation; ROS, reactive oxygen species; τ, overall time constant; [i]<sub>0</sub>, initial concentration of species *i*

### Introduction

#### Redox reactions and ROS in biological systems

Reactive oxygen species (ROS) (such as O<sub>2</sub><sup>•-</sup>, H<sub>2</sub>O<sub>2</sub> and organic hydroperoxides) are produced naturally in cells. They are signalling molecules, essential for

the normal metabolism of cells and tissues [1–3]. High levels of ROS will lead to a more oxidized redox environment thereby inducing cell damage or even cell death [4,5]. To protect against potential oxidative damage from these species, cells and tissues have a network of antioxidant enzymes to remove these ROS

Correspondence: V. G. J. Rodgers, Department of Bioengineering, University of California, Riverside, Riverside, CA 92521, USA. Tel: 1-951-827-6241. Fax: 1-951-827-5696. E-mail: victor.rodgers@ucr.edu

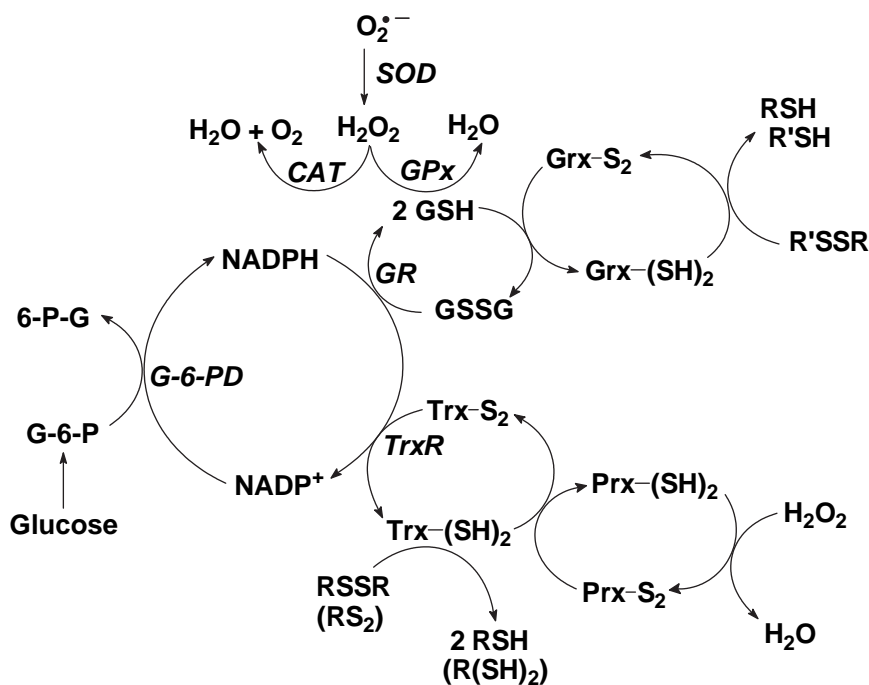


Figure 1. The hydrogen peroxide-removal system. There are at least three principal nodes for the removal of  $\text{H}_2\text{O}_2$ . Glutathione peroxidase (GPx) is a selenoenzyme that reduces  $\text{H}_2\text{O}_2$  to  $2\text{H}_2\text{O}$  gathering the needed reducing equivalents from glutathione (GSH). The peroxiredoxin (Prx) family of enzymes is a separate node, removing  $\text{H}_2\text{O}_2$  using reducing equivalents principally from thioredoxin (Trx). Catalase (CAT) is primarily located in peroxisomes; it requires no reducing cofactors to catalyse the disproportionation of  $\text{H}_2\text{O}_2$ .

(Figure 1). There are several families of enzymes that remove  $\text{H}_2\text{O}_2$ . This network has at least three nodes for peroxide-removal:

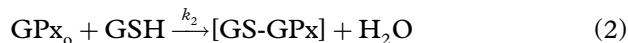
- Catalase is the longest known enzyme for removal of  $\text{H}_2\text{O}_2$ ; it requires no cofactors in its catalytic mode [6];
- the six members of the peroxiredoxin family of enzymes remove  $\text{H}_2\text{O}_2$  by reducing it to water and are in general recycled by gathering reducing equivalents from thioredoxin [7,8]; and
- the glutathione peroxidases rely on glutathione (GSH) for the necessary reducing equivalents.

This study focused only on the effects of GPx and GSH levels on  $\text{H}_2\text{O}_2$  removal, assuming the catalase and peroxiredoxin levels were unchanged.

#### GPx and GSH in removal of $\text{H}_2\text{O}_2$

In 1957 the family of glutathione peroxidases (GPx) was discovered [9]. Currently, at least four members of this family of enzymes are known [10–12]. They all reduce  $\text{H}_2\text{O}_2$  to water (organic hydroperoxides are reduced to water and the corresponding alcohol) with the electrons coming from GSH, a necessary and specific cofactor.

The kinetic behaviour of GPx-1 in dilute aqueous solution is best explained by a sequence of simple bimolecular reactions [13–15]:



yielding the overall reaction,



For bovine GPx-1, the kinetics of this reaction have been well studied and are considered to be a ‘ping-pong’ mechanism with indefinite Michaelis constants, indefinite maximum velocities and no significant product inhibition [10,16–22]. For this system the effective rate constants are given in Table I.

The observations in dilute, buffered solutions lead to the paradigm that in most circumstances, the rate of peroxide removal *in vivo* is essentially independent of the concentration of GSH [16,18,23]. This assumes low levels of  $\text{H}_2\text{O}_2$  (i.e.  $\text{H}_2\text{O}_2 < \text{GPx}_r < \text{GSH}$ ) and, thus, the rate of recycling of  $\text{GPx}_r$  by GSH (equations 2 and 3) is rapid compared to the rate of the reaction of  $\text{GPx}_r$  with  $\text{H}_2\text{O}_2$ . Thus, GPx would predominantly exist in its reduced form, which is highly reactive with hydroperoxides (equation 1).

Table I. Rate constants for modeling the kinetic behaviour of GPx [30].

Rate constant	( $\text{m}^{-1}\text{s}^{-1}$ )
$k_1$	$2.1 \times 10^7$
$k_2$	$4 \times 10^4$
$k_3$	$1 \times 10^7$

However, recent observations by Li et al. [24] in a cell culture model are not in agreement with the above paradigm. When human cytosolic GPx-1 cDNA was transfected into a set of MnSOD-over-expressing U118 cells (a glioma cell line), they observed that:

- The GSSG content of these cells had a linear direct relation to the product of (GPx activity)  $\times$  GSH, referred to as *effective GPx activity*. This is consistent with a higher rate of removal of  $H_2O_2$  leading to an increase in GSSG;
- Intracellular ROS (oxidation within the cell), as measured by the change in fluorescence of intracellular dichlorofluorescein, had a linear inverse relationship to effective GPx activity. This is consistent with a higher steady-state level of  $H_2O_2$  (Figure 2);
- The cell population doubling time had a linear inverse relationship to effective GPx activity, i.e. the greater the effective GPx activity, the faster the cells grew. This observation is coupled to the assumption that a higher effective GPx activity will lower the steady-state level of  $H_2O_2$  and lead

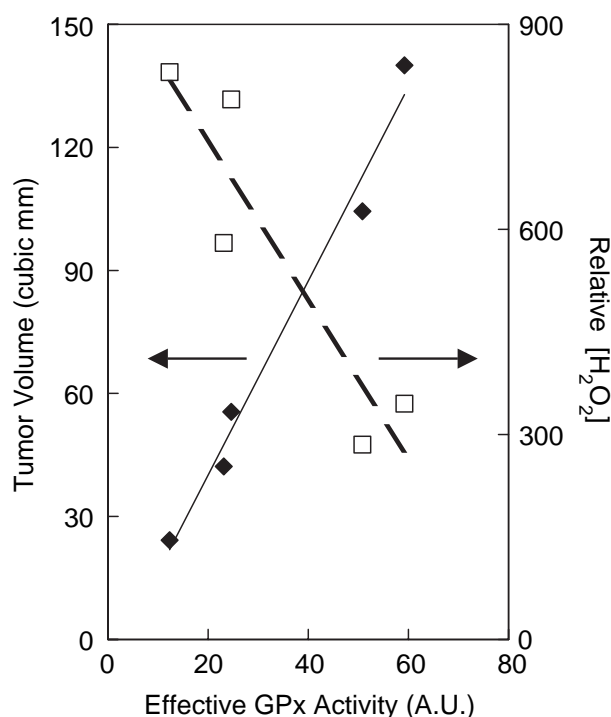


Figure 2. The rate of tumour growth *in vivo* varies directly with effective GPx activity (i.e. GPx  $\times$  GSH);  $H_2O_2$  varies inversely. (◆) Tumour volume, which is proportional to the growth rate. (□) Relative levels of intracellular  $H_2O_2$  were estimated by monitoring the increase in fluorescence of 2',7'-dichlorodihydrofluorescein (DCFH<sub>2</sub>). Effective GPx activity is 'GPx-activity' (or GPx) as measured by standard activity assay [44] multiplied by the concentration of GSH. The units are somewhat arbitrary (AU); using typical expressions of the activity of GPx (mU/mg protein) and for GSH levels (nmol/mg protein) units for effective GPx activity would be mU?nmol (mg protein)<sup>-2</sup>. Figure adapted from [55].

to a more reduced cellular redox environment and increased rate of growth [25]; and

- Most striking is that when the tumourigenicity of this set of cells with varying GPx activity was tested in nude mice, the growth rate of the tumours had a direct, linear relationship to effective GPx activity [24] (Figure 2). This is consistent with the *in vitro* observations, (a–c) above, and points to a fundamental role of  $H_2O_2$  in setting the biological status of cells and tissues [5,25].

In the above study of Li et al. [24], over-expression of MnSOD and genetic modifications with respect to GPx-1 resulted in higher fluxes of  $H_2O_2$  and various levels of GPx-1 in the cells. Because of the linear relationships with respect to [GPx][GSH] seen in Figure 2, these modifications appear not to have caused any significant changes in catalase or peroxiredoxin. Thus, the work of Li et al. serves as a reference for our modelling efforts to understand the GPx1-GSH- $H_2O_2$  system.

### Objective

The objective of this work is to examine the rate of removal of  $H_2O_2$  with respect to the kinetic rate behaviour of GPx-1 and GSH. Justification of the kinetic model is possible by using the *in vivo* observations of Li et al. [24] to: (1) determine when the rate-results from the kinetic models are consistent with the observed effective GPx activity dependency; and (2) estimate the probable range of average cellular GPx and  $H_2O_2$  in the cell lines investigated. To do this, we employed both the generalized and the classical approaches to express the kinetic rate behaviour involved in the GPx1-GSH- $H_2O_2$ -system (equations 1–3) and extract concentration dependency from the overall system time constant,  $\tau$  (also termed turnover time or biological 'average life' [26]). Finally, the variation of the classical model results from those of the general model was examined within this framework.

### Methods

#### Generalized mathematical description of the removal of $H_2O_2$ by GPx

Often in determining the rate of removal of hydrogen peroxide, the concentration of GSH is assumed to be constant [27]. Invoking this approximation and assuming spatial independence, the transient behaviour of species described by equations (1–3) are a set of non-linear ordinary differential equations (ODEs) that describe the rates of change in the concentration of each species, equations (5–10). Here  $C_i$  represents the concentration of species  $i$ .

$$\frac{dC_{GPx_r}}{dt} = k_3 C_{GSH} C_{GSGPx} - k_1 C_{GPx_r} C_{H_2O_2} \quad (5)$$

$$\frac{dC_{H_2O_2}}{dt} = -k_1 C_{GPx_r} C_{H_2O_2} \quad (6)$$

$$\frac{dC_{GPx_o}}{dt} = k_1 C_{GPx_r} C_{H_2O_2} - k_2 C_{GSH} C_{GPx_o} \quad (7)$$

$$\frac{dC_{H_2O}}{dt} = k_1 C_{GPx_r} C_{H_2O_2} + k_2 C_{GSH} C_{GPx_o} \quad (8)$$

$$\frac{dC_{GSGPx}}{dt} = k_2 C_{GSH} C_{GPx_o} - k_3 C_{GSH} C_{GSGPx} \quad (9)$$

$$\frac{dC_{GSSG}}{dt} = k_3 C_{GSH} C_{GSGPx} \quad (10)$$

From a mathematical viewpoint, the experimental observations of Li et al. [24] can now be compared to the concentration dependency of the rate of removal of  $H_2O_2$  for initial masses of  $H_2O_2$ , GPx and GSH introduced to the system (termed impulse response). These masses are described as equivalent initial concentrations. Since effective GPx activity proposed by Li et al. is the GPx activity coupled with GSH, we represent this as the product of initial  $GPx_r$  and GSH concentrations,  $[GPx_r]_0 \times [GSH]_0$ . This approximation is used to represent effective GPx activity for the purpose of investigating our kinetic rate models.

#### Classical approximation of the rate of removal of $H_2O_2$ by GPx

Because of the inherent non-linearity of the generalized expressions for the rate of removal of  $H_2O_2$ , a traditional kinetic rate law approximation (the classical model) is typically used. The classical model, in fact, is derived from the generalized rate expressions. Using a steady-state approximation, assuming that the enzyme concentration is lower than the substrate concentration, the rate of change of all substrate-enzyme intermediates are negligible, the relationship between the initial rate,  $v_0$ , total enzyme concentration,  $e$ , and initial substrate concentrations,  $S_i$ , for an enzymatic reaction with two substrates is approximated as [28]:

$$\frac{e}{v_0} = \frac{\Phi_1}{[S_1]} + \frac{\Phi_2}{[S_2]} \quad (11)$$

where  $\Phi_i$ 's are functions of reaction rate constants,  $k_i$ 's.

This approximation can be obtained from the general model (equations 5–10) by invoking several approximations for the kinetic rate model for the GPx1-GSH- $H_2O_2$  system. Starting with equations (5–10), by assuming constant concentrations of intermediates (equations 7 and 9, set to zero) and manipulating equation (6), one can obtain the classical rate expression for removal of  $H_2O_2$ , [16,29]:

$$\frac{[GPx_r]_0}{\frac{d[H_2O_2]}{dt}} = \frac{\Phi_1}{[H_2O_2]_0} + \frac{\Phi_2}{[GSH]_0}, \quad (12)$$

where,

$$\Phi_1 = \frac{1}{k_1} \quad (13)$$

And

$$\Phi_2 = \frac{1}{k_2} + \frac{1}{k_3}. \quad (14)$$

This classical expression results in a rate that is constant and depends only on the initial concentrations.

In this study, both the generalized and classical models are used to evaluate the rate of  $H_2O_2$  removal. A comparison of relevant similarities and differences are provided.

#### Parameters: Initial concentrations and reaction rate constants

In developing the model, we first need a range of concentrations that bracket expected physiological values. Using the data of Li et al. [24], we estimate the range of GSH in the five cell lines (Figure 2) to be 0.12–0.44 mM. Thus, we used the initial concentrations of 0.1–0.6 mM for GSH (Table II). However, there is no accurate way of correlating the data of Li et al. to  $GPx_r$  or  $H_2O_2$  concentrations; their initial concentrations are estimated from related literature values.

Most GPx is determined to be in its reduced form (> 99%) from both *in vivo* studies [18] and mathematical simulations [27]. Therefore, we assumed all GPx in our model to be initially in the reduced form,  $GPx_r$ . Estimated cellular concentrations of GPx vary from 0.2  $\mu M$  in red blood cells [18] to values of 2.5  $\mu M$  and 6.7  $\mu M$  derived from mathematical models [27,30]. Rat liver cytosolic GPx-1 has been estimated to be 5.8  $\mu M$  from Se of 0.46 ppm [31]; total GPx (monomer) in mitochondria and in the luminal space of endoplasmic reticulum is estimated to be 10  $\mu M$  and 0.32  $\mu M$ , respectively [32]. These values may be an over-estimate as we now know

Table II. Initial concentrations used for the GPx model.

Species	Initial concentration (m)
GSH	$1 \times 10^{-4}, 2 \times 10^{-4}, 4 \times 10^{-4}, 6 \times 10^{-4}$
$GPx_r$	$1 \times 10^{-7}, 5 \times 10^{-7}, 1 \times 10^{-6}, 5 \times 10^{-6},$ $1 \times 10^{-5}, 5 \times 10^{-5}$
$H_2O_2$	$1 \times 10^{-7}, 5 \times 10^{-7}, 1 \times 10^{-6}, 5 \times 10^{-6},$ $1 \times 10^{-5}, 5 \times 10^{-5}$
$GPx_o$	0
GS-GPx	0
GSSG	0

that there are additional Se-containing enzymes, e.g. thioredoxin reductase [33]. As suggested by the vast difference in reported concentrations, our initial  $GPx_r$  used in our modelling ranges from 0.1–50  $\mu\text{M}$  (Table II).

The concentration of  $\text{H}_2\text{O}_2$  in organisms can vary widely, from 0.2 nM in red blood cells to as high as 200  $\mu\text{M}$  in wound fluid [34,35]. Concentrations of  $\text{H}_2\text{O}_2$  in rat liver cells have been found to range from  $10^{-9}$ – $10^{-7}$  M [36]. A recent survey of intracellular  $[\text{H}_2\text{O}_2]$  has estimated 700 nM in non-pathological conditions [37]. This upper limit of 700 nM is suggested because intracellular levels above this value induce apoptosis in Jurkat T-cells [38]. Reportedly,  $\text{H}_2\text{O}_2$  was found to be able to reach 7  $\mu\text{M}$  in cytosol and 2  $\mu\text{M}$  in mitochondria [39]. To capture the higher level of  $\text{H}_2\text{O}_2$  due to the over-expression of MnSOD in the genetically-modified glioma cells used by Li et al. [24], the range of initial  $\text{H}_2\text{O}_2$  chosen for our model was varied from 0.1–50  $\mu\text{M}$  (Table II).

Rate constants for equations (1–3) have been determined in dilute buffer solutions [16,18,23]. These rate constants vary depending on conditions such as the buffer-salt and pH of the solution. Rate constants used (Table I) represent estimates of the effective intracellular rate constants for the three principal steps of the GPx catalytic cycle [30].

#### *Time constant for the removal of $\text{H}_2\text{O}_2$*

In order to search for ranges of possible physiological  $GPx_r$  and  $\text{H}_2\text{O}_2$  for cell lines under conditions used by Li et al. [24], time-dependent numerical solutions given by our model of the GPx1-GSH- $\text{H}_2\text{O}_2$  system are correlated to the observations of Li et al. As shown in Figure 2, the data of Li et al. present a linear relation between the effective GPx activity and the relative cellular  $\text{H}_2\text{O}_2$ . This biological observation can be compared to the concentration dependency of the rate of removal of  $\text{H}_2\text{O}_2$ . The dependency is generally reflected in an analytical solution for the overall system time constant,  $\tau$  (turnover time), provided that the model is linear. The overall rate by which the system evolves is dominated by this approximated time constant in the system. Thus, the functional dependency of  $\tau$  will allow us to understand the kinetic behaviour of the GPx1-GSH- $\text{H}_2\text{O}_2$  system.

However, because of the non-linearity of the rate equations associated with the removal of  $\text{H}_2\text{O}_2$  (due to the coupling of time-dependent concentrations of species in the terms on the right-hand side of each expression (equations 5–10), a closed-form solution does not exist. For non-linear systems,  $\tau$  can be approximated.

#### *Relating overall system time constant to effective GPx activity*

To meet our objectives, we have determined the dependency of effective GPx activity on  $\tau$  for the chosen range of initial GSH,  $GPx_r$  and  $\text{H}_2\text{O}_2$  concentrations. Specifically, this is when  $\tau$  is inversely proportional to effective GPx activity, consistent with the observations of Li et al. [24],

$$\tau \propto \frac{1}{C_{GSH}C_{GPx_r}}. \quad (16)$$

Then, comparing these values to acceptable physiological conditions for the genetically-modified cells used by Li et al. [24], we will pose possible ranges of average cellular GPx and  $\text{H}_2\text{O}_2$ .

The initial conditions for variables held constant are shown in Table II. There are six initial concentrations used for  $\text{H}_2\text{O}_2$ ,  $[\text{H}_2\text{O}_2]_0$ , in our models. For every  $[\text{H}_2\text{O}_2]_0$ , there are six different initial concentrations used for  $GPx_r$ ,  $[GPx_r]_0$ . Similarly, for each  $[GPx_r]_0$  there are four initial concentrations used for GSH,  $[GSH]_0$ . This results in 144 cases for each general and classical model.

The time constant,  $\tau$ , of interest here is the time taken for a 63% decay in  $\text{H}_2\text{O}_2$ . For the general model,  $\tau$  for removal of  $\text{H}_2\text{O}_2$  can be extracted from the numerical solutions of the generalized rate expressions (equations 5–10). Since the rate of removal of  $\text{H}_2\text{O}_2$  given by the classical approach is independent of time,  $\tau$  can be directly calculated by integrating equation (12).

#### *Numerical methods*

All equation-sets were solved with initial concentrations and rate constants, listed in Tables I and II. Species rate expressions, shown in equation (5–10), are therefore numerically integrated by using the IMSL (International Mathematical and Statistical Library) DIVPAG (double-precision initial value problem solver using either Adam-Moulton's or Gear's method) coded using Fortran [40–42].

## **Results and discussion**

#### *Mathematical ranges of concentrations demonstrating effective GPx activity dependency*

In Figure 3 are plotted values of all  $\tau$  obtained from both the general and classical models, organized for each  $[\text{H}_2\text{O}_2]_0$ , v the values of  $[GPx_r]_0$  and  $[GSH]_0$  on a log-log scale. Time constants from the general model for  $[\text{H}_2\text{O}_2]_0$  of 0.1–50  $\mu\text{M}$  are shown as solid lines in Figure 3(A–F). In each figure panel, corresponding to a given  $[\text{H}_2\text{O}_2]_0$ ,  $[GPx_r]_0$  ranges from 0.1–50  $\mu\text{M}$ , shown with various colours. For each  $[GPx_r]_0$  there are four  $[GSH]_0$  (0.1, 0.2, 0.4 and 0.6 mM) that make up each line. In Figure 3(a), the reaction starts with  $[\text{H}_2\text{O}_2]_0$  of 0.1  $\mu\text{M}$ . As expected, for cases where

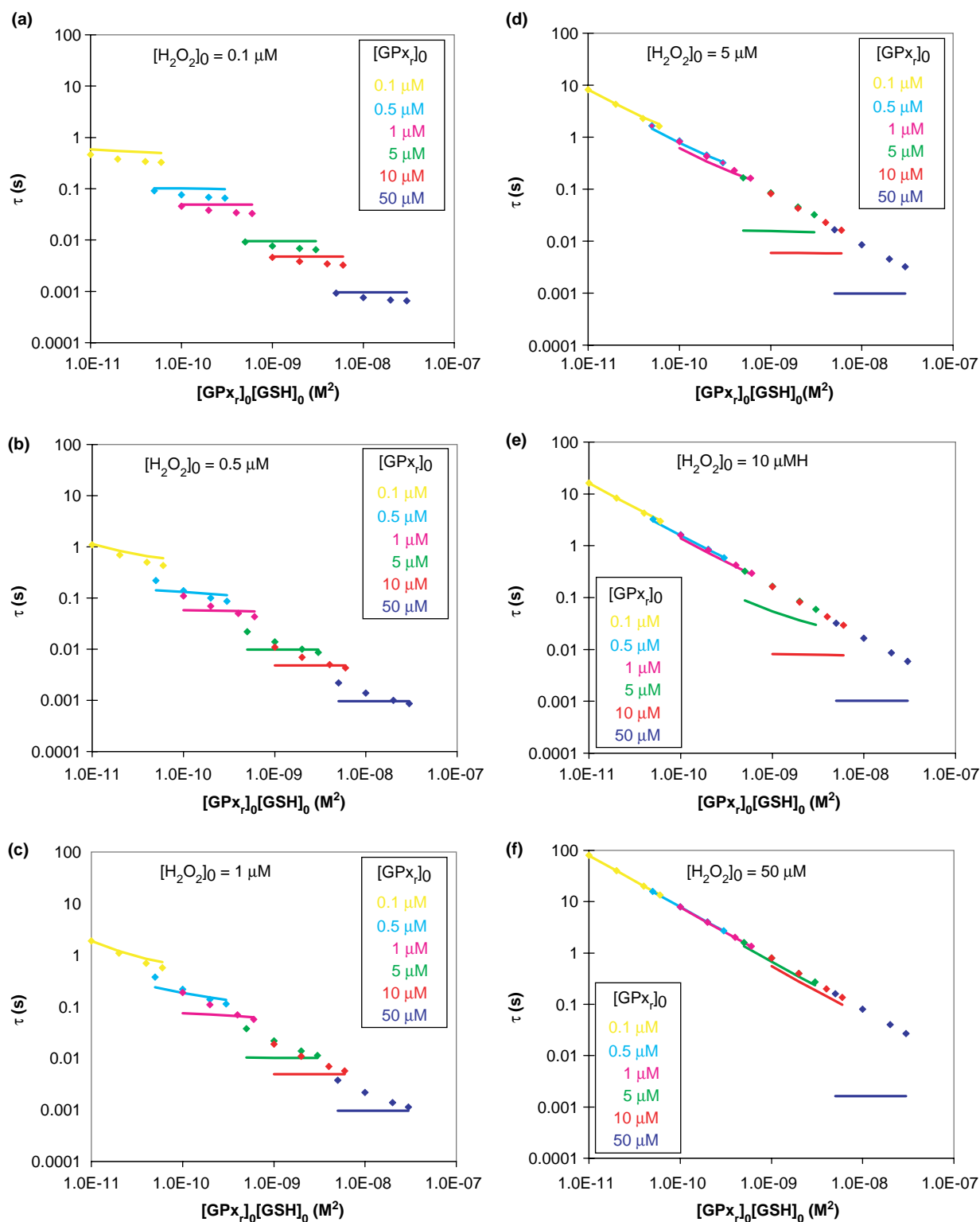


Figure 3. Model results in determining linear dependency of time constant with respect to effective GPx activity. The dependence of the time constant,  $\tau$ , on effective GPx activity, approximated by  $[GPx_r]_0[GSH]_0$ , are shown on log-log plots for various initial concentrations of GPx<sub>r</sub> and H<sub>2</sub>O<sub>2</sub>. Results from the general model are shown as solid lines; results from the classical model are shown as dotted lines. The short segments result from calculations of effective GPx activity for a fixed  $[GPx_r]_0$  with a span on  $[GSH]_0$  (0.1, 0.2, 0.4 and 0.6 mM). If the line segments are parallel to the abscissa, then there is no dependence of  $\tau$  on  $[GSH]$  in the range of concentrations tested; if the line segments show a non-zero slope, then there is dependence of  $[GSH]$ . The system would be completely dependent on effective GPx activity if all points fell on a single straight line.  $[GPx_r]_0$  used for both models are 0.1  $\mu M$ , 0.5  $\mu M$ , 1  $\mu M$ , 5  $\mu M$ , 10  $\mu M$  and 50  $\mu M$ . (a)  $[H_2O_2]_0 = 0.1 \mu M$ ; (b)  $[H_2O_2]_0 = 0.5 \mu M$ ; (c)  $[H_2O_2]_0 = 1 \mu M$ ; (d)  $[H_2O_2]_0 = 5 \mu M$ ; (e)  $[H_2O_2]_0 = 10 \mu M$ ; (f)  $[H_2O_2]_0 = 50 \mu M$ . The general model captures dependency when  $[H_2O_2]_0$  is 5  $\mu M$  and  $[GPx_r]_0$  is  $\leq 1 \mu M$ . Note that the classical model under-predicts the  $[H_2O_2]_0$  for the onset of effective GPx activity dependency. Furthermore, the estimated time constants for the classical model can be orders of magnitude different than that determined from the more general kinetic model.

$[\text{GPx}_r]_0 > [\text{H}_2\text{O}_2]_0$ , there is no GSH dependency;  $\tau$  is inversely proportional to  $[\text{GPx}_r]_0$  only. When the system starts with equal amounts of  $[\text{GPx}_r]_0$  and  $[\text{H}_2\text{O}_2]_0$ ,  $\tau$  begins to show both  $\text{GPx}_r$ -dependency and slight GSH-dependency for cases with lower  $[\text{GSH}]_0$ . Similar trends are observed as  $[\text{H}_2\text{O}_2]_0$  increases, as seen in Figure 3(b–f).

There is little or no GSH-dependency on  $\tau$  when  $[\text{GPx}_r]_0 > [\text{H}_2\text{O}_2]_0$ . This clearly shows that the rate of removal of  $\text{H}_2\text{O}_2$  is not a function of  $[\text{GSH}]_0$ . In these cases,  $\tau$  is inversely proportional to  $[\text{GPx}_r]_0$ ; therefore, the system's ability to remove  $\text{H}_2\text{O}_2$  is not affected by the recycling of  $\text{GPx}_r$  or the amount of GSH available.

Only when  $[\text{GPx}_r]_0 \leq [\text{H}_2\text{O}_2]_0$  does  $\tau$  begin to show dependency on both  $[\text{GPx}_r]$  and  $[\text{GSH}]$ , i.e. the time needed for removal of  $\text{H}_2\text{O}_2$  increases and is clearly a function of both  $[\text{GPx}_r]_0$  and  $[\text{GSH}]_0$ . The removal of  $\text{H}_2\text{O}_2$  in these cases depends on the continuous recycling of  $\text{GPx}_r$  and the amount of GSH available to recycle  $\text{GPx}_r$  becomes important. These results are in agreement with the analysis of Flohé and colleagues [16,18,19]. It is generally believed that  $[\text{GPx}_r] > [\text{H}_2\text{O}_2]$  in cells and tissues. However, both the observations of Li et al. [24] and our kinetic model imply that these conditions are not always true.

Based on our generalized mathematical model, there exist sets of initial  $\text{GPx}_r$  and GSH concentrations within all ranges studied where  $\tau$  is generally inversely proportional to  $[\text{GPx}_r]_0[\text{GSH}]_0$  for the removal of  $\text{H}_2\text{O}_2$ , agreeing with the findings of Li et al. [24] shown in Figure 2 and the relationship expressed in Equation (16). This linear relationship between  $\tau$  and  $[\text{GPx}_r]_0[\text{GSH}]_0$  is clearly visible for the following cases:

1. When  $[\text{H}_2\text{O}_2]_0$  is 5, 10 and 50  $\mu\text{M}$ , as shown in Figure 3(d–f), for  $[\text{GPx}_r]_0$  of 0.1, 0.5 and 1  $\mu\text{M}$ ; and,
2. When  $[\text{H}_2\text{O}_2]_0$  is 50  $\mu\text{M}$ , as shown in Figure 3(F), for  $[\text{GPx}_r]_0$  of 0.1, 0.5, 1, 5 and 10  $\mu\text{M}$ .

#### *Implications of modelling results relative to the observed biological phenomena*

Mathematical modelling demonstrates that the rate of removal of  $\text{H}_2\text{O}_2$  can be a function of  $[\text{GPx}_r]_0[\text{GSH}]_0$ , specifically when  $[\text{GPx}_r]_0 < [\text{H}_2\text{O}_2]_0$  and the recycling of  $\text{GPx}_r$  is rate-limiting. Assuming the rate of production of  $\text{H}_2\text{O}_2$  is on the same order as the rate of removal, varying  $[\text{GPx}_r]_0[\text{GSH}]_0$  would change the steady-state level of  $\text{H}_2\text{O}_2$ . This is consistent with Li et al.'s [24] observations. When the U118 cells of Li et al. were genetically manipulated to change  $[\text{GPx}_r]_0[\text{GSH}]_0$ , the apparent steady-state level of  $\text{H}_2\text{O}_2$  varied inversely with  $[\text{GPx}_r]_0[\text{GSH}]_0$ . The *in vivo* observations presented in Figure 2 clearly

demonstrate that effective  $\text{GPx}$  activity ( $[\text{GPx}_r]_0[\text{GSH}]_0$ ) correlates with biochemical and biological properties. Most striking is that this is associated with the rate of growth for tumours. Thus, effective  $\text{GPx}$  activity appears to be an important biochemical parameter to monitor and use to understand the biology associated with differing fluxes of  $\text{H}_2\text{O}_2$  and the role of the peroxide-removing system.

Although the rate of elimination of  $\text{H}_2\text{O}_2$  *in vivo* by  $\text{GPx}$  is generally assumed to be independent of  $[\text{GSH}]$ , the results of the kinetic simulation indicated that the rate of peroxide-removal can potentially be a function of  $[\text{GSH}]$ . To help explain this we have to address the range of initial concentrations ( $[\text{GPx}]_0$ ,  $[\text{GSH}]_0$ ,  $[\text{H}_2\text{O}_2]_0$ ) used, which are estimated from the U118 cells of Li et al. [24]. Reported levels of GSH and activities of  $\text{GPx}$  of other cells are compared with those of the U118 cells.

Typical levels of GSH in cells range from 1–10 mM [25]. From the data of Li et al. [24] on the level of GSH in U118 cells and a cellular volume of 2.4 pL (F.Q. Schafer, unpublished), we estimated the range of GSH in the five cell lines of Figure 2 to be 0.12–0.44 mM. This is 10-times smaller than concentrations typically observed in proliferating cells.

The measured activity of  $\text{GPx}$  in the set of cells studied ranged from 15–65 mU/mg protein (using the assay and unit definition of [43]).  $[\text{GPx}]$  is considered to be at lower levels in tumour cells and cancer [6,44–48]. These values are comparable to the range of values published for other cancer cell lines, e.g. PC-3 cells, 18 mU/mg protein [49]; MCF-7, 38 mU/mg protein; MDA-MB231, 98 mU/mg protein; and MCF-10A, 218 mU/mg protein [50]. These comparisons point to the low levels of GSH in U-118 cells as being a contributor to Li et al.'s [24] observation that peroxide levels and tumour growth are a function of ( $\text{GPx}$  activity)  $\times$   $[\text{GSH}]$ .

The time constant results provided by the general model indicate that if the possible intracellular concentration of  $\text{H}_2\text{O}_2$  is in the range of 5–50  $\mu\text{M}$ , then the physiological concentration of  $\text{GPx}$  is likely to be between 0.1–10  $\mu\text{M}$ . However, as mentioned above, the upper limit for intracellular  $[\text{H}_2\text{O}_2]$  in normal cells is proposed to be  $\sim 700$  nM [37,38]. However, the genetically-modified glioma cells used by Li et al. [24] over-expressed MnSOD by as much as 5-fold. This increase in MnSOD will likely increase the steady-state concentration of  $\text{H}_2\text{O}_2$  [1]. Therefore, a predicted physiological range of  $[\text{H}_2\text{O}_2]$  and  $[\text{GPx}_r]$  for the results of Li et al. are approximately  $[\text{GPx}_r] \leq 1$   $\mu\text{M}$  and  $[\text{H}_2\text{O}_2] \sim 5$   $\mu\text{M}$ .

It should be noted that actual concentrations may vary from those proposed by our model. This is because the modelling results are a consequence of the selected reaction rate constants and initial concentrations used in Equations (1–3).

Finally, it is important to recognize that, in our modelling of the removal of  $\text{H}_2\text{O}_2$  by the GPx-GSH- $\text{H}_2\text{O}_2$  system, spatially dependent concentrations were not considered and cellular averages were used. However, gradients in the intracellular concentrations clearly exist [6,37,51] and can result in local dominance of the rate of removal of  $\text{H}_2\text{O}_2$  that can alter our predicted cellular average concentrations.

#### *Deviations of the classical model from the general model results*

Time constants obtained from the classical model for  $[\text{H}_2\text{O}_2]_0$  in the range of 0.1–50  $\mu\text{M}$  are also shown in Figure 3(a–f) as dots representing all cases studied. Unlike the general model,  $\tau$  shows dependency on both  $[\text{GPx}_r]$  and  $[\text{GSH}]$  for the entire range of concentrations tested. Linear dependency of  $\tau$  on  $[\text{GPx}_r]_0[\text{GSH}]_0$  can be observed when  $[\text{H}_2\text{O}_2]_0$  varies from 1–50  $\mu\text{M}$  for  $[\text{GPx}_r]_0$  of 0.1–50  $\mu\text{M}$  (Figure 3(c–f)). Although the resulting values for  $\tau$  from the classical model deviate noticeably from the general model for most cases, they agree within the probable physiological ranges of  $[\text{GPx}_r]$  and  $[\text{H}_2\text{O}_2]$  suggested by the general model. This behaviour occurs as a result of the assumptions in the classical model that the enzyme concentration is lower than that of the substrate. Therefore, under this condition of relatively low  $[\text{GPx}_r]$  and high  $[\text{H}_2\text{O}_2]$ , both models should agree well, especially for the low  $[\text{GSH}]$  found for U118 cells.

However, due to simplifications made in deriving the classical rate expression, the classical model is less sensitive in capturing the full behaviour of the removal of cellular  $\text{H}_2\text{O}_2$ . Using the case where  $[\text{H}_2\text{O}_2]_0$  is 5  $\mu\text{M}$  and  $[\text{GSH}]_0$  is 0.1 mM, transient  $[\text{H}_2\text{O}_2]$  profiles for both the general (solid lines) and classical (dotted lines) models are presented on a semi-log plot (Figure 4(a)). The  $[\text{H}_2\text{O}_2]$  from the classical model is calculated by integrating the rate expression shown in Equation (12). The time taken for 63% decay (which is  $\sim \tau$ ) in both models agrees relatively well for the three cases where  $[\text{GPx}_r]_0$  is 0.1, 0.5 and 1  $\mu\text{M}$  (as also shown in Figure 3(d)). For example, in the case where  $[\text{GPx}_r]_0$  is 1  $\mu\text{M}$ , although  $\tau$ 's given for both models are close, the times predicted for 10% decay by the two models are more than an order of magnitude different. The rates of removal of  $\text{H}_2\text{O}_2$  at 1 ms given by the two models, as shown in Figure 4(B), are two orders of magnitude different. These differences, which occur early during reactions, could result in substantial cumulative discrepancies.

Furthermore, for the same case, the  $\text{H}_2\text{O}_2$  profile given by the classical model does not capture the inflection point where there is an obvious change in the rate of removal of  $\text{H}_2\text{O}_2$ . The slower rate of  $\text{H}_2\text{O}_2$  removal is due to the slow recycling of GPx, as shown

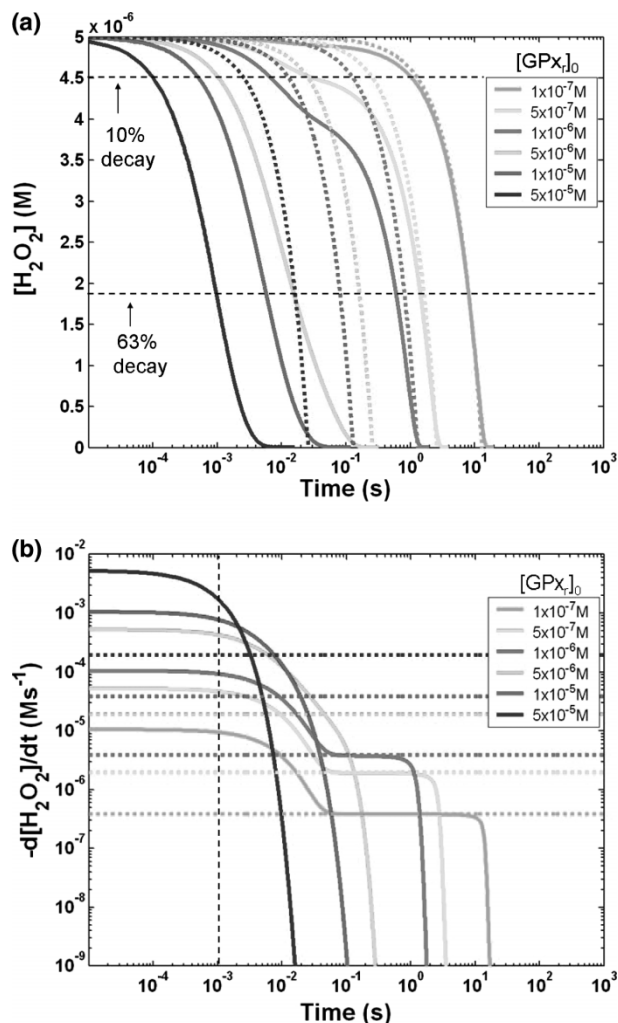


Figure 4. Example cases demonstrating deviations between the generalized and classical model results. Cases used here, as examples to demonstrate discrepancies, are for initial concentration of  $\text{H}_2\text{O}_2$ ,  $[\text{H}_2\text{O}_2]_0$ , of 5  $\mu\text{M}$  and initial concentration of GSH,  $[\text{GSH}]_0$ , of 0.1 mM. (A) Transient  $\text{H}_2\text{O}_2$  profiles for various  $[\text{GPx}_r]_0$  of the general (solid lines) and classical (dotted lines) models are shown in this semi-log plot. Even for cases with lower  $[\text{GPx}_r]_0$ , where the time needed for 63% decay (time constants,  $\tau$ ) from both models agree well, the classical model is not a good approximation throughout. For example, in the case where  $[\text{GPx}_r]_0$  is 1  $\mu\text{M}$  (magenta), the time taken for 10% decay given by both models are a factor of 10 different. (b) The rates of disappearance of  $\text{H}_2\text{O}_2$  for various  $[\text{GPx}_r]_0$  of the general (solid lines) and classical (dotted lines) models are plotted with a semi-log scale. Using the same case of where  $[\text{GPx}_r]_0$  is 1  $\mu\text{M}$  (magenta), at physiological turnover time for  $\text{H}_2\text{O}_2$  of ms, the rate of removal of  $\text{H}_2\text{O}_2$  given by the general model is approximately a factor of 100 greater than the classical rate.

in a plot comparing the transient  $[\text{H}_2\text{O}_2]$  and  $[\text{GPx}_r]$  (Figure 5). These points of inflection are clearly visible for cases where  $[\text{GPx}_r]_0 < [\text{H}_2\text{O}_2]_0$  (Figure 4(a)). When  $[\text{H}_2\text{O}_2]$  is initially higher than  $[\text{GPx}_r]$ , then  $[\text{GPx}_r]$  is the rate-limiting factor. When this is the case, the continuation of the  $\text{H}_2\text{O}_2$ -eliminating reaction of Equation (1) depends on the amount of  $\text{GPx}_r$  being recycled. This is particularly true when

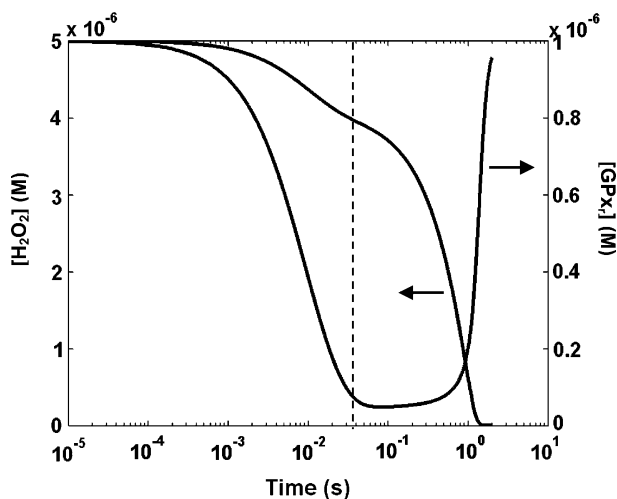


Figure 5. Example of the rate-limiting effect of the slower  $\text{GPx}_r$  recycling step. Concentration profiles of  $\text{H}_2\text{O}_2$  and  $\text{GPx}_r$  of the general model are shown for  $[\text{H}_2\text{O}_2]_0$  of  $5 \mu\text{M}$ ,  $[\text{GSH}]_0$  of  $0.1 \text{ mM}$  and  $[\text{GPx}_r]_0$  of  $1 \mu\text{M}$ . The inflection point on the  $[\text{H}_2\text{O}_2]$ -profile that occurs around  $40 \text{ ms}$  corresponds to the change in the rate of production of  $\text{GPx}_r$ .

the recycling reaction steps, shown in equations (2) and (3), are much slower compared to the  $\text{H}_2\text{O}_2$ -eliminating step. The reaction rate constant for Equation (2) is three orders of magnitude smaller than the rate constant for equation (1); the rate constant for Equation (3) is very near that of equation (1). Thus, Equation (2) would be a rate-limiting reaction in the recycling of  $\text{GPx}_r$ . In cases with lower  $[\text{GPx}_r]$  and  $[\text{GSH}]$ , the slow recycling effect becomes more significant at earlier times during the process.

Nevertheless, these discrepancies are based on the set of initial concentrations used, as illustrated in Figure 4(B). Using the same example where  $[\text{H}_2\text{O}_2]_0$  is  $5 \mu\text{M}$  and  $[\text{GSH}]_0$  is  $0.1 \text{ mM}$ , for cases with  $[\text{GPx}_r]_0$  of  $0.1$ ,  $0.5$  and  $1 \mu\text{M}$ , there exists a steady-state region for the rate of removal of  $\text{H}_2\text{O}_2$  given by the general model. This steady-state rate is concurrent to steady-state  $[\text{GPx}_o]$  and  $[\text{GS-GPx}]$ . Since the classical rate expression is derived by invoking the steady-state approximation on  $\text{GPx}_o$  and  $\text{GS-GPx}$ , the rate given by the classical model should be in agreement with this steady-state rate given by the general model, as seen in Figure 4(b).

Finally, modelling the removal of  $\text{H}_2\text{O}_2$  by the  $\text{GPx-GSH-H}_2\text{O}_2$  system is a multi-scale problem and is spatially dependent. The time scale for removal of  $\text{H}_2\text{O}_2$  is on the order of milliseconds [27,52] whereas cell growth is on the order of days. Therefore, small differences in modelling solutions could significantly impact long-term predicted behaviour. For this reason, the classical approach to expressing the rate of enzymatic reactions should be used with caution, especially when addressing more complex systems.

## Conclusions

With the use of kinetic modelling, we have investigated the removal of  $\text{H}_2\text{O}_2$  by  $\text{GPx}$ . Our goal was to examine the concentration dependency of intracellular  $\text{H}_2\text{O}_2$  removal to understand the anomalies in the findings of Li et al. [24]. They observed that biochemical parameters related to the removal of  $\text{H}_2\text{O}_2$  in genetically-modified U118-9 cells were a function of effective  $\text{GPx}$ -activity; most striking was their observation that the rate of tumour growth in an animal model was directly related to effective  $\text{GPx}$  activity. Using mathematical modelling, with sets of reaction rate constants and initial species concentrations taken from the literature, we found that:

- as expected, the rate of removal of  $\text{H}_2\text{O}_2$  increased with  $[\text{GPx}_r]_0$ ;
- the rate of removal of  $\text{H}_2\text{O}_2$  is affected by  $[\text{GPx}_r]_0$  and  $[\text{GSH}]_0$  when  $[\text{GPx}_r]_0 < [\text{H}_2\text{O}_2]_0$ ; the reason for this is the slow recycling of  $\text{GPx}_r$ ;
- the overall time constant,  $\tau$ , is inversely proportional to the product  $[\text{GPx}_r]_0 \times [\text{GSH}]_0$ , as shown in equation (16); this holds for intracellular concentrations of  $\text{GPx}_r \leq 1 \mu\text{M}$  with  $[\text{H}_2\text{O}_2] \geq 5 \mu\text{M}$  and for  $\text{GPx}_r \leq 10 \mu\text{M}$  with  $[\text{H}_2\text{O}_2] \geq 50 \mu\text{M}$ ;
- the plausible concentrations for U118 cells of Li et al. [24] are predicted to be  $\sim \text{GPx}_r \leq 1 \mu\text{M}$  and  $[\text{H}_2\text{O}_2] \sim 5 \mu\text{M}$ ;
- the classical approach to deriving the rate of removal of  $\text{H}_2\text{O}_2$ , as expressed in equation (12), matches the generalized rate favourably when species concentrations corresponding to steady-state  $[\text{GPx}_o]$  and  $[\text{GS-GPx}]$  are used;
- but, while offering useful simplicity, under certain conditions, the classical approach can result in substantial differences from the more general form over long time periods.

In the future, to further examine this system, the current lumped parameter mathematical model should be refined to include spatial dependency and  $\text{H}_2\text{O}_2$  generation. Issues of transport properties, such as species diffusivities and membrane permeability, and reaction rate constants, perhaps due to the crowded environment [53,54], need to be investigated. A direct coupling of cell growth to  $\text{H}_2\text{O}_2$  residence time is required to connect mathematical simulation to biological observations.

Mathematical modelling made it possible to quantitatively study the time constants (turnover time) associated with the removal of  $\text{H}_2\text{O}_2$  by  $\text{GPx}$ , providing insight into a biological observation that could not be approached experimentally. Finally, modelling demonstrates that the paradigm established from the kinetic-observations in dilute aqueous

buffer do not always hold in the complex milieu of the cell.

### Acknowledgement

This investigation was supported by the National Institutes of Health Grants CA-84462, and CA-66081.

### References

- [1] Buettner GR, Ng CF, Wang W, Rodgers VGJ, Schafer FQ. A new paradigm: manganese superoxide dismutase influences the production of H<sub>2</sub>O<sub>2</sub> in cells and thereby their biological state. *Free Radic Biol Med* 2006;41:1338–1350.
- [2] Liu R, Buettner GR, Oberley LW. Oxygen free radicals mediate the induction of manganese superoxide dismutase gene expression by TNF- $\alpha$  in human oral carcinoma SCC-25 cells. *Free Radic Biol Med* 2000;28:1197–1205.
- [3] Oberley LW, Oberley TD, Buettner GR. Cell division in normal and transformed cells: the possible role of superoxide dismutase and hydrogen peroxide. *Med Hypotheses* 1981;7:21–42.
- [4] Jones DP. Extracellular redox state: refining the definition of oxidative stress in aging. *Rejuvenation Res* 2006;9:169–181.
- [5] Jones DP. Disruption of mitochondrial redox circuitry in oxidative stress. *Chem-Biol Interact* 2006;163:38–53.
- [6] Chance B, Sies H, Boveris A. Hydroperoxide metabolism in mammalian organs. *Physiol Rev* 1979;59:527–605.
- [7] Rhee SG, Chang TS, Bae YS, Lee SR, Kang SW. Cellular regulation by hydrogen peroxide. *J Am Soc Nephrol* 2003;14(8 Suppl 3):S211–S215.
- [8] Rhee SG, Chae HZ, Kim K. Peroxiredoxins: a historical overview and speculative preview of novel mechanisms and emerging concepts in cell signaling. *Free Radic Biol Med* 2005;38:1543–1552.
- [9] Mills GC. Hemoglobin catabolism. I. Glutathione peroxidase, an erythrocyte enzyme which protects hemoglobin from oxidative breakdown. *J Biol Chem* 1957;229:189–197.
- [10] Ursini F, Maiorino M, Brigelius-Flohé R, Aumann KD, Roveri A, Schomburg D, Flohé L. Diversity of glutathione peroxidases. *Methods Enzymol* 1995;252:38–53.
- [11] Brigelius-Flohé R. Tissue-specific functions of individual glutathione peroxidases. *Free Radic Biol Med* 1999;27:951–965.
- [12] Brigelius-Flohé R, Winkler R, Muller C. Estimation of individual types of glutathione peroxidases. *Methods Enzymol* 2002;347:101–112.
- [13] Schneider F, Flohé L. Untersuchungen über glutathion-H<sub>2</sub>O<sub>2</sub>-oxydoreduktase (Glutathion-Peroxidase). *Hoppe-Seylers Zeitschrift Fur Physiologische Chemie* 1967;348:540–552.
- [14] Flohé L, Schaich E, Voelter W, Wendel A. Glutathion peroxidase. 3. Spectral characteristics and experiments on reaction mechanism. *Hoppe-Seylers Zeitschrift Fur Physiologische Chemie* 1971;352:170–180.
- [15] Flohé L. Glutathione peroxidase—enzymology and biological aspects. *Klinische Wochenschrift* 1971;49:669–683.
- [16] Flohé L, Loschen G, Gunzle WA, Eichele E. Glutathione peroxidase, V. The kinetic mechanism. *Hoppe-Seylers Zeitschrift fur Physiologische Chemie* 1972;353:987–999.
- [17] Maiorino M, Roveri A, Gregolin C, Ursini F. Different effects of Triton X-100, deoxycholate, and fatty acids on the kinetics of glutathione peroxidase and phospholipid hydroperoxide glutathione peroxidase. *Arch Biochem Biophys* 1986;251:600–605.
- [18] Flohé L. Glutathione peroxidase: fact and fiction. *Ciba Foundation Symp* 1978;65:95–122.
- [19] Gunzler WA, Vergin H, Muller I, Flohé L. Glutathione peroxidase VI: the reaction of glutathione peroxidase with various hydroperoxides. *Hoppe-Seylers Zeitschrift fur Physiologische Chemie* 1972;353:1001–1004.
- [20] Ursini F, Maiorino M, Gregolin C. The selenoenzyme phospholipid hydroperoxide glutathione peroxidase. *Biochim Biophys Acta* 1985;839:62–70.
- [21] Esworthy RS, Chu FF, Geiger P, Girotti AW, Doroshow JH. Reactivity of plasma glutathione peroxidase with hydroperoxide substrates and glutathione. *Arch Biochem Biophys* 1993;307:29–34.
- [22] Aumann KD, Bedorf N, Brigelius-Flohé R, Schomburg D, Flohé L. Glutathione peroxidase revisited—simulation of the catalytic cycle by computer-assisted molecular modeling. *Biomed Environ Sci* 1997;10:136–155.
- [23] Salvador A, Antunes F, Pinto RE. Kinetic modeling of in vitro lipid peroxidation experiments—‘low level’ validation of a model of *in vivo* lipid peroxidation. *Free Radic Res* 1995;23:151–172.
- [24] Li S, Yan T, Yang JQ, Oberley TD, Oberley LW. The role of cellular glutathione peroxidase redox regulation in the suppression of tumor cell growth by manganese superoxide dismutase. *Cancer Res* 2000;60:3927–3939.
- [25] Schafer FQ, Buettner GR. Redox state of the cell as viewed through the glutathione disulfide/glutathione couple. *Free Radic Biol Med* 2001;30:1191–1212.
- [26] Mawson CA. Meaning of ‘turnover’ in biochemistry. *Nature* 1955;176:317.
- [27] Antunes F, Salvador A, Marinho S, Alves R, Pinto RE. Lipid peroxidation in mitochondrial inner membranes. I. An integrative kinetic model. *Free Radic Biol Med* 1996;21:917–943.
- [28] Dalziel K. Initial steady state velocities in the evaluation of enzyme-coenzyme-substrate reaction mechanisms. *Acta Chem Scand* 1957;11:1706–1723.
- [29] Forstrom JW, Stults FH, Tappel AL. Rat liver cytosolic glutathione peroxidase: reactivity with linoleic acid hydroperoxide and cumene hydroperoxide. *Arch Biochem Biophys* 1979;193:51–55.
- [30] Antunes F, Salvador A, Pinto RE. PHGPx and phospholipase A<sub>2</sub>/GPx: comparative importance on the reduction of hydroperoxides in rat liver mitochondria. *Free Radic Biol Med* 1995;19:669–677.
- [31] Stults FH, Forstrom JW, Chiu DTY, Tappel AL. Rat liver glutathione peroxidase: purification and study of multiple forms. *Arch Biochem Biophys* 1977;183:490–497.
- [32] Marinho HS, Antunes F, Pinto RE. Role of glutathione peroxidase and phospholipid hydroperoxide glutathione peroxidase in the reduction of lysophospholipid hydroperoxides. *Free Radic Biol Med* 1997;22:871–883.
- [33] Liu SY, Stadtman TC. Heparin-binding properties of selenium-containing thioredoxin reductase from HeLa cells and human lung adenocarcinoma cells. *Proc Natl Acad Sci USA* 1997;94:6138–6141.
- [34] Giulivi C, Hockstein P, Davies KJA. Hydrogen peroxide production by red blood cells. *Free Radic Biol Med* 1994;16:123–129.
- [35] Roy S, Khana S, Nallu K, Hunt TK, Sen SK. Dermal wound healing is subject to redox control. *Molecular Therapy* 2006;13:211–220.
- [36] Oshino N, Chance B, Sies H, Bucher T. The role of H<sub>2</sub>O<sub>2</sub> generation in perfused rat liver and the reaction of catalase compound I and hydrogen donors. *Arch Biochem Biophys* 1973;154:117–131.

- [37] Stone JR. An assessment of proposed mechanisms for sensing hydrogen peroxide in mammalian systems. *Arch Biochem Biophys* 2004;422:119–124.
- [38] Antunes F, Cadenas E. Cellular titration of apoptosis with steady state concentrations of H<sub>2</sub>O<sub>2</sub>: submicromolar levels of H<sub>2</sub>O<sub>2</sub> induce apoptosis through Fenton chemistry independent of the cellular thiol state. *Free Radic Biol Med* 2001;30:1008–1018.
- [39] Antunes F, Cadenas E. Estimation of H<sub>2</sub>O<sub>2</sub> gradients across biomembranes. *FEBS Lett* 2000;475:121–126.
- [40] Gear CW. Numerical initial-value problems in ordinary differential equations. Englewood Cliffs, NJ: Prentice-Hall; 1971.
- [41] Hindmarsh AC. GEAR: Ordinary differential equation system solver. Lawrence Livermore Laboratory. Report UCID-30001. Revision 3; 1974.
- [42] User's Manual. Differential equations. In: The IMSL Libraries. Version 2.0. Houston, Texas: IMSL Inc; 1991. p 755–771.
- [43] Lawrence RA, Burk RF. Glutathione peroxidase activity in selenium-deficient rat liver. *Biochem Biophys Res Commun* 1976;71:952–958.
- [44] Oberley LW, Buettner GR. The role of superoxide dismutase in cancer: a review. *Cancer Res* 1979;39:1141–1149.
- [45] Sun Y, Oberley LW, Elwell JH, Sierra-Rivera E. Antioxidant enzyme activities in normal and transformed mouse liver cells. *Int J Cancer* 1989;44:1028–1033.
- [46] Hardman WE, Munoz J Jr, Cameron IL. Role of lipid peroxidation and antioxidant enzymes in omega 3 fatty acids induced suppression of breast cancer xenograft growth in mice. *Cancer Cell Int* 2002;2:10.
- [47] Yang J, Lam EWN, Hammad HM, Oberley TD, Oberley LW. Antioxidant enzyme levels in oral squamous cell carcinoma and normal human oral epithelium. *J Oral Pathol Med* 2002;31:71–77.
- [48] Hu YJ, Dolan ME, Bae R, Yee H, Roy M, Glickman R, Kiremidjian-Schumacher L, Diamond AM. Allelic loss at the GPx-1 locus in cancer of the head and neck. *Biol Trace Elem Res* 2004;101:97–106.
- [49] Venkataraman S, Jiang X, Weydert CJ, Zhang Y, Zhang HJ, Goswami PC, Ritchie JM, Oberley LW, Buettner GR. Manganese superoxide dismutase overexpression inhibits the growth of androgen-independent prostate cancer cells. *Oncogene* 2005;24:77–89.
- [50] Weydert CJ, Waugh TA, Ritchie JM, Iyer KS, Smith JL, Li L, Spitz DR, Oberley LW. Overexpression of manganese or copper zinc superoxide dismutase inhibits breast cancer growth. *Free Radic Biol Med* 2006;41:226–237.
- [51] Makino N, Sasaki K, Hashida K, Sakakura Y. A metabolic model describing the H<sub>2</sub>O<sub>2</sub> elimination by mammalian cells including H<sub>2</sub>O<sub>2</sub> permeation through cytoplasmic and peroxisomal membranes: comparison with experimental data. *Biochim Biophys Acta* 2004;1673:149–159.
- [52] Reth M. Hydrogen peroxide as second messenger in lymphocyte activation. *Immunology* 2002;3:1129–1134.
- [53] Schnell S, Turner TE. Reaction kinetics in intracellular environments with macromolecular crowding: simulations and rate laws. *Prog Biophys Molec Biol* 2004;85:235–260.
- [54] Hanggi P, Talkner P, Borkovec M. Reaction-rate theory—50 years after Kramers. *Rev Mod Phys* 1990;62:251–341.
- [55] Li SJ. The role of cellular glutathione peroxidase redox regulation in the suppression of tumor cell growth by manganese superoxide dismutase [dissertation]. Iowa City (IA): University of Iowa; 1999. Available from The University of Iowa, Iowa City, IA.